

Accepted Manuscript

Numerical simulation of bias and photo stress on indium-gallium-zinc-oxide thin film transistors

M. Adaiika, Af Meftah, N. Sengouga, M. Henini

PII: S0042-207X(15)00173-6

DOI: [10.1016/j.vacuum.2015.04.021](https://doi.org/10.1016/j.vacuum.2015.04.021)

Reference: VAC 6640

To appear in: *Vacuum*

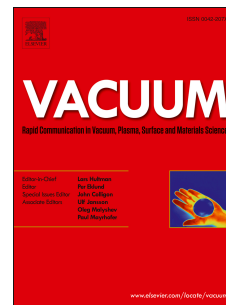
Received Date: 1 November 2014

Revised Date: 30 March 2015

Accepted Date: 10 April 2015

Please cite this article as: Adaiika M, Meftah A, Sengouga N, Henini M, Numerical simulation of bias and photo stress on indium-gallium-zinc-oxide thin film transistors, *Vacuum* (2015), doi: 10.1016/j.vacuum.2015.04.021.

This is a PDF file of an unedited manuscript that has been accepted for publication. As a service to our customers we are providing this early version of the manuscript. The manuscript will undergo copyediting, typesetting, and review of the resulting proof before it is published in its final form. Please note that during the production process errors may be discovered which could affect the content, and all legal disclaimers that apply to the journal pertain.



Numerical simulation of bias and photo stress on indium-gallium-zinc-oxide thin film transistors

M.Adaika¹, Af.Meftah¹, N.Sengouga^{1,*}, and M.Henini²

¹Laboratoire des Matériaux Semiconducteurs et Métalliques (LMSM), Université de Biskra, B.P.145, 07000 Biskra, Algeria

²School of Physics and Astronomy, Nottingham Nanotechnology and Nanoscience Center, University of Nottingham, NG7 2RD, UK

*Corresponding author: n.sengouga@univ-biskra.dz (N Sengouga), Tel/Fax +213 33

54 31 99

Abstract.

Thin Film Transistors based on amorphous Indium-Gallium-Zinc-Oxide (a-IGZO TFT) are receiving a great deal of attention for their numerous applications as alternatives for amorphous and poly-crystalline Silicon based TFTs. A major concern about a-IGZO TFTs is that they suffer from instabilities when subjected to different types of stress (bias, light, etc...). Stress is believed to create defects of different kinds in different regions of the device. The instability manifests as a shift in the threshold voltage or a hump in the transfer characteristics of the transistor. In addition, there is still a great deal of confusion about the relation between defects and the instability induced by stress. The main purpose of this study is to elucidate the relation between the threshold voltage shift (instability) and the defects created by stress. For this purpose a detailed numerical simulation was carried out to investigate the relation between the different types of defects created by stress and the induced instability in a-IGZO TFT. It was found that tail, deep and interface states cause a shift in threshold

voltage. Negative and positive shifts are observed if the defects are donor-like and acceptor-like defects, respectively. On the other hand, a hump in the transfer characteristics is induced if discrete interface levels are dominant.

Keywords: IGZO; TFT; bias stress; optical stress; defects; SILVACO simulation.

1 Introduction

Thin film transistors (TFTs) are used in numerous electronics applications such as active matrix organic light emitting diodes (AMOLED), active matrix liquid crystal display (AMLCD) [1,2], and fast circuits [3]. Although several materials such as amorphous silicon (a-Si), polycrystalline silicon (pc-Si) and organic semiconductors (OS) can be used as active layers for TFTs, there has been growing interest in amorphous oxide semiconductors (AOS) based on zinc oxide (ZnO) such as indium-gallium-zinc oxide (IGZO) [4]. a-Si and OS TFTs have a low field-effect mobility while pc-Si TFTs suffer from non-uniformity over large areas [5]. IGZO TFTs have several advantages which include visible light transparency [6], large-area uniform deposition at low temperature [7], good controllability of carrier concentration [5] and high carrier mobility [8]. However, the threshold voltage of a-IGZO TFTs, like in other TFTs, can be severely degraded by different types of stress such as negative or positive bias, temperature, exposure to light or even mechanical strain [9,10]. This phenomenon is referred to as threshold voltage instability. It is believed that stress induced instability is due to defects created in different regions of the device. Lopes et al [11] reported that the origin of the threshold voltage instability is due to the charge trapping at residual-water-related trap sites following a gate voltage stress. Liu et al [12] related the shift in the electrical characteristics after a negative gate bias (NGBS) prolonged stress to the degradation of the contact between source/drain and a-IGZO

active layer. The distribution of states in the conduction band can also be affected by a prolonged bias stress [13]. Light stress also induces threshold shift [14] which is related to the capture of photo-induced hole carriers by donor-like interface traps. Dao et al [15] related the threshold instability to carrier trapping rather than defect creation after the device was subjected to a prolonged gate bias stress. A hump may also appear in the electrical characteristics of a-IGZO TFTs subjected to a large positive gate bias stress [16]. Deep states above the valence band, created by constant current stress and negative bias stress at the surface of a-IGZO under illumination, may also be responsible for the instability [17]. The degradation mechanism of a-IGZO TFTs under positive gate bias and negative gate bias with illumination are attributed to electron and hole trapping, respectively, at the insulator-channel interface [18]. The exposure of an a-IGZO TFT to ultraviolet radiation induces a negative shift in its electrical characteristics despite that no bias stress is applied [19]. This shift is explained by the ionization of neutral oxygen vacancies in the active layer. It was also observed that negative bias enhances the shift while positive bias reduces it. Jeon et al [20] found that illuminated a-IGZO TFTs showed stable characteristics under positive gate bias stress but a huge shift in the threshold voltage under negative gate bias stress. In this case it is believed that hole trapping in the gate dielectric layer is the major cause of this degradation. In order to elucidate the difference between bias and illumination stress, Vemuri et al [21] showed that excessive positive gate bias stress creates charge trap states while light with wavelengths below 532 nm create ionised vacancies. Although there were several attempts to reduce instability following different types of stress such as temperature annealing, addition of a buffer layer, and chemical treatment, the phenomenon still persists.

It is therefore evident that there are a lot of non-clarified issues related to the effect of different means of stress on the electrical characteristics of a-IGZO TFTs. In particular what kind of stress (optical, gate bias, drain bias, temperature, etc.) creates which of defects (interface, bulk, discrete levels, continuous DOS, etc).

This work is an attempt to investigate a specific side of this issue. In particular it will be assumed that a stress, whatever its nature is, will create either an interface defect between the active channel (a-IGZO thin film) and the dielectric material, a bulk defect in the active channel (as a Gaussian acceptor or increase the initial Gaussian donor) or a bulk defect in the dielectric. The transfer characteristics of the a-IGZO TFT under these different assumptions are numerically calculated using the SILVACO TCAD software [22]. Numerical simulation has the unique feature that the effect of different parameters can be studied independently or simultaneously. This, obviously, cannot be achieved by experimental work or analytical modelling.

2. The a-IGZO TFT structure

A two dimensional cross section along the channel of the a-IGZO TFT structure used in this work is shown in figure 1 which is a staggered bottom-gate similar to that of reference [23]. The channel is 20 nm thick a-IGZO, the substrate is a heavily doped n-type poly-silicon which also acts as a gate, the gate insulator is a 100 nm thick SiO₂ layer, the drain and source Ohmic contacts are 5 μm long low resistance titanium (Ti). The separation between the source and drain is 30 μm.

The channel is made of a-IGZO which is an amorphous n-type semiconductor. Its structural properties are adapted from those of amorphous hydrogenated silicon (a-

Si:H) [24]. Disordered materials (like a-Si and a-IGZO) contain a large number of defect states continuously distributed within the band gap of the material. The density of states is a combination of exponentially decaying band tail states and Gaussian distributions of mid-gap states.

The conduction band-tail (CB) states (acceptor-like states $g_{ct}^A(E)$) are given by exponential function decay:

$$g_{ct}^A(E) = g_{ta} \exp\left(\frac{E - E_C}{E_a}\right)$$

Where $g_{ta} (cm^{-3} eV^{-1})$ is the effective density at E_C , and E_a is the characteristic slope energy of the conduction band-tail states.

The valence band-tail (VB) states (donor-like states $g_{vt}^D(E)$) are also given by a similar expression:

$$g_{vt}^D(E) = g_{td} \exp\left(\frac{E_V - E}{E_a}\right)$$

Where $g_{td} (cm^{-3} eV^{-1})$ is the effective density at E_V , and E_a is the characteristic slope energy of the valence band-tail states.

In addition to tail states, Gaussian-distributed donor-like and acceptor-like defect states, $g_G^D(E)$ and $g_G^A(E)$, respectively, in the energy gap are also considered

$$g_G^D(E) = g_{ga} \exp\left(-\frac{(E - E_D)^2}{\sigma_D^2}\right)$$

$$g_G^A(E) = g_{ga} \exp\left(-\frac{(E_A - E)^2}{\sigma_A^2}\right)$$

Where g_{gd} (g_{ga}), are the total density ($cm^{-3}eV^{-1}$), σ_D (σ_A) the standard deviation and E_D (E_A) the peak energy of the Gaussian distribution. The schematic DOS in amorphous semiconductors is shown in Figure 2.

For a-IGZO, the conduction band minimum (CBM) is mainly made of the empty s orbitals of the metal cation and the valence band maximum (VBM) is of fully occupied O-2p orbitals [25]. CBMs of oxides are made of spherically spread s orbitals of metal cations, and their overlaps with neighboring metal s orbitals are not altered largely by disordered amorphous structures. Therefore, electronic levels of CBM are less sensitive to local strained bonds [26], while, the O-2p orbitals have various directions in amorphous oxides due to the disorder of the amorphous structure. This accounts for the origin of the p orbital localization and the valence band tail states. In addition, this explains the reason why the VB tail states have a wider distribution compared to the CB tail states which are very narrow [27].

The energy levels of oxygen vacancies (VO), that is, the non-bonding state of the metal cation, is formed in or near the CBM allowing the vacancies to act as a shallow donor but not as an effective electron trap. It should be noted that such donor states are not stable in many oxides. Even in such cases, the oxygen vacancy level is relaxed to form a fully occupied deep state, which no longer traps an electron and is inactive for electron transport in n-channel TFTs [28, 29]. These deep states explain why a-IGZO TFTs do not show an inversion operation because the high-density occupied states in the band gap pin the Fermi level when the TFTs are subjected to a negative gate bias. They also inhibit to induce mobile holes in the VB [28]. A high-density subgap states exist also below the CBM. They act as electron traps, pin the Fermi

level when a positive gate bias is applied, and deteriorate the TFT operation [28, 30-33]

Since the IGZO thin film is an n-type semiconductor and the IGZO TFT is operated in the accumulation mode, in our simulation the DOS is modeled by the tail states and the donor-like deep states only, i.e. neglecting the acceptor like deep Gaussian states [23].

3. Numerical simulation

In order to characterise semiconductor devices and elucidate the observed effects to each other, extensive experimental work and/or analytical or qualitative modelling has to be carried out. Experimental characterisation is time consuming and can be very expensive, and analytical modelling may have non-physical meaning. Numerical simulation can help in both cases: reduce the cost and time needed for experimentation and is physically based approach. For this purpose ATLAS of SILVACO, a physically- based two and three dimensional device simulator is used. It predicts the electrical behavior of specified semiconductor structures by using the well-established Drift-Diffusion Model [34]. This model is based on the Poisson's and continuity equations. The Poisson's equation which relates the electronic potential to the space charge density is given by:

$$\text{div}(\epsilon \nabla \psi) = -\rho = -q(p - n + n_{tail} - p_{tail} + n_{ga} - p_{gd} + N_d) \quad (1)$$

Where ψ is the electrostatic potential, ϵ is the local permittivity, ρ is the local space charge density, n and p are the free carrier's densities, N_d is the n-channel doping concentration and n_{tail} , p_{tail} , n_{ga} , p_{gd} (the DOS constituents) are given by:

$$n_{tail} = \int_{E_V}^{E_C} g_{ct}^A(E) f_{ct}^n(E) dE$$

$$p_{tail} = \int_{E_V}^{E_C} g_{vt}^D(E) f_{vt}^p(E) dE$$

$$n_{ga} = \int_{E_V}^{E_C} g_G^A(E) f_{AG}^n(E) dE$$

$$p_{gd} = \int_{E_V}^{E_C} g_G^D(E) f_{DG}^p(E) dE$$

Where $f_{ct}^n(E)$, $f_{AG}^n(E)$ are the ionization probabilities of the acceptor tail and Gaussian states, respectively, and $f_{vt}^p(E)$, $f_{DG}^p(E)$ are the ionization of the donor states (tail and Gaussian). At the steady state, these ionization probabilities are given by the Shockley-Read-Hall (SRH) model [33-34]:

$$f_{ct}^n(E) = \frac{v_{th}^n \sigma_{nc} n + v_{th}^p \sigma_{pc} n_i e^{\frac{E_i - E}{k_B T}}}{v_{th}^n \sigma_{nc} \left(n + n_i e^{\frac{E - E_i}{k_B T}} \right) + v_{th}^p \sigma_{pc} \left(p + n_i e^{\frac{E_i - E}{k_B T}} \right)}$$

$$f_{AG}^n(E) = \frac{v_{th}^n \sigma_{ng}^a n + v_{th}^p \sigma_{pg}^a n_i e^{\frac{E_i - E}{k_B T}}}{v_{th}^n \sigma_{ng}^a \left(n + n_i e^{\frac{E - E_i}{k_B T}} \right) + v_{th}^p \sigma_{pg}^a \left(p + n_i e^{\frac{E_i - E}{k_B T}} \right)}$$

$$f_{vt}^p(E) = \frac{v_{th}^p \sigma_{pv} p + v_{th}^n \sigma_{nv} n_i e^{\frac{E - E_i}{k_B T}}}{v_{th}^n \sigma_{nc} \left(n + n_i e^{\frac{E - E_i}{k_B T}} \right) + v_{th}^p \sigma_{pc} \left(p + n_i e^{\frac{E_i - E}{k_B T}} \right)}$$

$$f_{DG}^p(E) = \frac{v_{th}^p \sigma_{pg}^d p + v_{th}^n \sigma_{ng}^d n_i e^{\frac{E - E_i}{k_B T}}}{v_{th}^n \sigma_{ng}^d \left(n + n_i e^{\frac{E - E_i}{k_B T}} \right) + v_{th}^p \sigma_{pg}^d \left(p + n_i e^{\frac{E_i - E}{k_B T}} \right)}$$

Where v_{th}^n is the electron thermal velocity and v_{th}^p is the hole thermal velocity, n_i is the intrinsic carrier concentration. σ_{nc} and σ_{ng}^a are the electron capture cross-section for the acceptor tail and Gaussian state, respectively. σ_{pc} and σ_{pg}^a are the hole capture cross-section for the acceptor tail and Gaussian states, respectively, and σ_{nv} , σ_{ng}^d , σ_{pv} and σ_{pg}^d are the equivalents for donor states.

The continuity equations for both electrons and holes, in steady state, are expressed as:

$$0 = \frac{1}{q} \text{div} \vec{J}_n + G_n - R_n \quad (2.a)$$

$$0 = -\frac{1}{q} \text{div} \vec{J}_p + G_p - R_p \quad (2.b)$$

Where \vec{J}_n and \vec{J}_p are the electron and hole current densities, G_n and G_p are the generation rates for electrons and holes which are neglected in this study, R_n and R_p are the total recombination rates for electrons and holes in Gaussian and tail states, and q is the electron charge. R_n and R_p are assumed to be the same and given by [35]

$$\begin{aligned}
R_n = R_p = & \int_{E_V}^{E_C} (np \\
& - n_i^2) \left\{ \left[\frac{v_{th}^n v_{th}^p \sigma_{pc} \sigma_{nc} g_{ct}^A(E)}{v_{th}^n \sigma_{nc} \left(n + n_i e^{\frac{E-E_i}{k_B T}} \right) + v_{th}^p \sigma_{pc} \left(p + n_i e^{\frac{E_i-E}{k_B T}} \right)} \right] \right. \\
& + \left[\frac{v_{th}^n v_{th}^p \sigma_{pv} \sigma_{nv} g_{vt}^D(E)}{v_{th}^n \sigma_{nc} \left(n + n_i e^{\frac{E-E_i}{k_B T}} \right) + v_{th}^p \sigma_{pv} \left(p + n_i e^{\frac{E_i-E}{k_B T}} \right)} \right] \\
& + \left[\frac{v_{th}^n v_{th}^p \sigma_{pg}^a \sigma_{ng}^a g_G^A(E)}{v_{th}^n \sigma_{ng}^a \left(n + n_i e^{\frac{E-E_i}{k_B T}} \right) + v_{th}^p \sigma_{pg}^a \left(p + n_i e^{\frac{E_i-E}{k_B T}} \right)} \right] \\
& \left. + \left[\frac{v_{th}^n v_{th}^p \sigma_{pg}^d \sigma_{ng}^d g_G^D(E)}{v_{th}^n \sigma_{ng}^d \left(n + n_i e^{\frac{E-E_i}{k_B T}} \right) + v_{th}^p \sigma_{pg}^d \left(p + n_i e^{\frac{E_i-E}{k_B T}} \right)} \right] \right\} dE
\end{aligned}$$

In the drift-diffusion model, the current densities are expressed in terms of the quasi-Fermi levels ϕ_n and ϕ_p as:

$$\vec{J}_n = -q\mu_n n \nabla \phi_n \quad (3.a)$$

$$\vec{J}_p = -q\mu_p p \nabla \phi_p \quad (3.b)$$

Where μ_n and μ_p are the electron and hole mobilities, respectively. The quasi-Fermi levels are linked to the carrier concentrations and the potential through $n =$

$$n_i \exp\left(\frac{\psi - \phi_n}{k_B T}\right) \text{ and } p = n_i \exp\left(-\frac{\psi - \phi_p}{k_B T}\right) \text{ where } n_i \text{ is the effective intrinsic}$$

concentration and T is the lattice temperature.

The electrical characteristics are calculated following the specified physical structure and bias conditions. This is achieved by approximating the operation of the device onto a two dimensional grid, consisting of a number of grid points called nodes. By applying the set of differential equation (Poisson's and continuity equations) onto this grid, the transport of carriers through the structure can be simulated. The finite element grid is used to represent the simulation domain. Of interest to the present work, the current-voltage characteristics are calculated under different conditions (type of defects created by bias and/or light stress).

4. Results and discussion

Stress definitely creates new defects or enhances existing ones as reported by numerous papers and explained in details in the introduction section [12, 14-16, 18-22]. The main issue is that no work has been carried out to clarify in which region of the devices these defects are created. The suggested locations of these defects are just hypotheses and can be anywhere in the different regions of the device: the bulk insulator, the bulk semiconductor or at the interface between them. Furthermore their spatial distribution may be uniform or have a complex shape. Their energetic distribution is also another issue. They can be discrete levels or have a Gaussian distribution. In simulating the relation between threshold voltage shift in a-IGZO TFTs bias and/or optical stress, several cases may therefore be considered.

In the present work we have only considered the most common cases. First, stress can enhance the fixed charge in the bulk insulator dielectric (SiO_2). The second case is when defects created by stress are at the interface between the insulator and the semiconductor. Finally stress induced defects which are uniformly distributed in the

bulk of the semiconductor (a-IGZO). Obviously, several other cases may arise and these are discussed in details later.

Before stress is considered and due to the amorphous nature of a-IGZO, we have assumed that the DOS in the pre-stressed TFT is modeled by tail states and a donor-like Gaussian distribution near CB tail while the acceptor-like Gaussian distribution near the VB is neglected. This choice is justified by the n-type nature of a-IGZO [23]. The parameters of this model are presented in Table 1.

Before presenting the simulation results for the different cases and in order to explain the observed effects of the different types of defects, it is worth to briefly describe the operation principle of an a-IGZO TFT. In an ideal n-type a-IGZO, when a positive bias is applied to the gate, an accumulation regime is created and with a positive drain-source applied voltage, the current flows in the channel. This is the ON regime of the TFT. The OFF regime is obtained by a negative bias of the gate which induces, in the channel, a region depleted of free electrons.

In a stressed a-IGZO TFT, by bias or other means, additional defect states are induced. If these states are acceptor-like then they will shift the threshold voltage (boundary voltage between accumulation regime and depletion regime) to the positive biases. While if the stress induced defects are donor-like, they will delay the depletion regime by shifting the threshold voltage to negative biases.

4.1. The fixed charge in the oxide:

The first considered is when stress creates an additional fixed charge in the insulator dielectric (SiO_2). We assume that the variable is the density of the fixed charge which

is practically related to the stress time. Figure 3 shows the TFT transfer characteristics (the drain-source current versus the gate voltage) for increasing charge density. The threshold voltage shifts to more negative values. In order to explain the shift in the threshold voltage, the band diagram of the semiconductor-insulator interface is plotted in figure 4. This bias value of $V_g = 1.15 V$ is the threshold voltage of the initial state. As the density of the fixed charge increases, the n-type density of the semiconductor increases indicating a displacement of the Fermi level towards the conduction band. This requires a more negative voltage to switch the transistor OFF. Thus the shift of the threshold voltage occurs at greater negative values.

4.2. Interface states:

Several authors have reported that the interface between the insulator and the semiconductor may be affected when the transistor is subjected to a bias; optical or other types of stress [11, 13]. These defects may be discrete levels or have a continuous distribution in the forbidden band gap.

4.2.1. Discrete levels:

The energy of the discrete levels created by stress is assumed to be an acceptor situated 0.4 eV from the bottom of the conduction band. Its density is a variable parameter which is also in direct relation to the stress time. Other parameters are shown in table 2. The effect of increasing the density of this discrete level is shown in figure 5. The curves exhibit a notable decrease of turn-on current with a hump-like shape. The results show that discrete traps between oxide and semiconductor, $\text{SiO}_2/\text{a-}$

IGZO, do not cause any shift of the curve but affects the turn-on current only. The band diagram will not be presented in this case since there is no shift in the threshold voltage.

4.2.2. Gaussian distribution:

Obviously in this case the defects may behave like acceptor or donor like for electrons. Therefore the two cases are considered. The parameters of the Gaussian interface states are given in table 3. Figure 6 presents the transfer characteristics of the TFT for the case when the defects created by stress behave like acceptors and donors (a and b, respectively). The threshold voltage shifts to greater positive values for the acceptor-like traps and to greater negative voltage for the donor-like defects in order to explain the shift in the threshold voltage, the band diagram of the semiconductor-insulator interface is plotted in figure 7 and 8, respectively. As the density of the interface defect increases the n-type density of the semiconductor decreases, indicating a shift of the Fermi level away from the conduction band. In (b) the semiconductor actually is almost in the intrinsic regime. This requires a more positive voltage to switch the transistor OFF, thus the shift of the threshold voltage to greater positive values. As the density of the interface defect increases, the n-type density of the semiconductor increases causing the Fermi level to more closer to the conduction band. This requires a more negative voltage to switch the transistor OFF, hence the shift of threshold voltage to greater negative values.

4.3 The midgap density of state (DOS)

This is perhaps the most probable case of all as proposed by many authors [36]. The midgap Gaussian states are affected by stress. Again two cases are considered. The first case is when the existing donor-like states are increased by stress. The second case is when acceptor-like states are newly generated by stress. It is worth pointing out that these states are neglected in the unstressed TFT as reported by most of previous work [5, 23, 32]. The parameters used in simulating the effect of Gaussian distributed defects in the gap of the semiconductor on the TFT transfer characteristics are summarised in table 4. The transfer characteristics of the TFT are represented in figure 9 when stress creates acceptor- and donor-like (a and b, respectively) deep Gaussian defects in the band gap of the semiconductor. The threshold voltage shifts to larger positive and negative values for the acceptor- and donor-like traps, respectively. The shift in the threshold voltage can be explained by plotting the band diagram of the semiconductor-insulator interface. These plots are shown in figures 10 and 11, respectively. As the density of deep defects increases the n-type concentration of the semiconductor decreases indicated a larger separation between the Fermi level and the conduction band. This requires a larger positive voltage to switch the transistor OFF, thus the shift of the threshold voltage to greater positive values. Similarly when the density of the deep defect increases, the n-type of the semiconductor decreases causing the Fermi level to be more distant from the conduction band. This requires a large negative voltage to switch the transistor OFF, hence the shift of the threshold voltage to greater negative values.

5. Conclusion

The SILVACO TCAD software was used to carry out a detailed numerical analysis for the purpose of elucidating the relation between the types of defects created by stress and the shift of the threshold voltage in an $-IGZO$ TFT. Stress can create several types of defects. They can be discrete levels or continuously distributed in the gap of the $a-IGZO$ semiconductor. They may be also at the semiconductor-insulator interface or even in the insulator itself. All these cases were considered. Wherever they are located (in real or energy space) they act as traps and/or recombination states. Hence they may affect the doping density as compensating or enhancing centers. Other parameters such as the lifetime of free carriers may be affected. It was found that acceptor-like defects induce a positive shift in the TFT threshold voltage while donor-like defects result in a negative shift of the threshold voltage. The exception is that interface discrete levels do not cause a threshold voltage shift but a hump in the transfer characteristics. The importance of this study lies the fact that it can elucidate the uncertainties in explaining why some types of stress induce positive shift, others negative shift and some cause none. In summary, deep, ail and interface states always cause a shift in the threshold voltage (negative if they are donor-like and positive if they are acceptor-like defects) while discrete interface levels just produce a hump in the transfer characteristics. In other word, if for example a positive shift in the threshold is experimentally observed then acceptor-like defects creation by stress dominates the donor-like defects. If just a hump is observed after stress then discrete interface creation dominates the other types of defects. When the fixed charge density increase from 10^{10} to 10^{12} cm^{-2} the threshold voltage shifts from -2 to -6 V . If the interface states are discrete levels and their density increase from 10^{12} to $10^{14} \text{ cm}^{-3} \text{ eV}^{-1}$ the threshold voltage does not shift but a hump is observed the I-V characteristics and the saturation current decreases substantially from micro-amps to

pico-amps. However if the interface states have Gaussian distributions and their density increases from 10^{10} to $10^{12} \text{ cm}^{-3} \text{ eV}^{-1}$ the threshold voltage is positively shifted from -2 to 2 V if they are acceptors while it shifts negatively from -2 to -6 V if they are donors. The midgap states have the greatest effect; if their density increases from 10^{15} to $10^{18} \text{ cm}^{-3} \text{ eV}^{-1}$ the threshold voltage is positively shifted from -2 to 6 V if they are acceptors while it shifts negatively from -2 to -10 V if they are donors.

6. References

- [1] Barquinha P, Martins R, Pereira L. *Transparent Oxide Electronics From Materials to Devices*. Chichester: John Wiley and Sons, 2012.
- [2] Mativenga M, Choi M, H, Choi J, W, Jang J. Transparent flexible Circuits Based on Amorphous-Indium-Gallium-Zinc-Oxide Thin Film Transistors. *IEEE Electron Dev Lett* 2011; 32:170-2.
- [3] Ofuji M, Abe K, Shimizu H, Kaji N, Hayashi R, Sano M, Kumomi H, Nomura K, Kamiya T, Hosono H. Fast Thin-Film Transistor Circuits Based on Amorphous Oxide Semiconductor. *IEEE Electron Dev Lett* 2007; 28(): 273-5.
- [4] Park JS, Maeng WJ, Kim HS, Park JS. Review of recent developments in amorphous oxide semiconductors thin-film transistor devices. *Thin Solid Films* 2012; 520: 1679-93.
- [5] Nomura K, Takagi A, Kamiya T, Ohta H, Hirano M, Hosonok H. Amorphous Oxide Semiconductors for High-Performance Flexible Thin-Film Transistors. *Jap J Appl Phys* 2006; 45: 4303-8.

- [6] Nomura K, Ohta H, Takagi A, Kamiya T, Hirano M, Hoson H. Room-temperature fabrication of transparent flexible thin-film transistors using amorphous oxide semiconductors *Nature* 2004; 432: 488-92.
- [7] Lee M, Dho J. Controlling the Electrical and the Optical Properties of Amorphous IGZO Films prepared by Using Pulsed Laser Deposition. *J. Korean Phys. Soc* 2011; 58: 492-7.
- [8] Hsu H, Cheng C, Chiou P, Chiu Y, Chang C, Zheng Z. Amorphous bilayer TiO₂-InGaZnO thin film transistors with low drive. *Solide-States Electronics* 2014; 99: 51-4.
- [9] Cheng HC, Tsay CY. Flexible a-IZO thin film transistors fabricated by solution processes. *J Alloys Compounds* 2010; 507: L1-3.
- [10] Jeong JK, Chung HJ, Mo YG, Kim HD. Comprehensive Study on the Transport Mechanism of Amorphous Indium-Gallium-Zinc Oxide Transistor. *J Electrochemical Society* 2008; 155: H873-7.
- [11] Lopes ME, Gomes HL, Medeiros M CR, Barquinha P, Pereira L, Fortunato E. Gate-bias stress in amorphous oxide semiconductors thin-film transistors. *Appl Phy Lett* 2009; 95: 063502.
- [12] Liu KH, Chang TC, Chang KC, Tsai TM, Hsieh TY, Chen MC. Investigation of on-current degradation behaviour induced by surface hydrolysis effect under negative gate bias stress in amorphous InGaZnO thin-film transistor. *Appl Phy Lett* 2014; 104: 103501.

- [13] Mathews WP, Vemuri RNP, Alford TL. Influence of Extended Bias Stress on the Electrical Parameters of Mixed Oxide Thin Film Transistors. *Circuits and Systems* 2012; 3: 295-9.
- [14] Lee SY, Song SM, Song MK, Lee WG, Yoon KS, Kwon JY. The Light Response Characteristics of Oxide-Based Thin Film Transistors. *World Academy of Science, Engineering and Technology* 2011; 5: 511-4.
- [15] Dao VA,, Trinh TT,, Jang K,, Ryu K, Yi J. Trapping Time Characteristics of Carriers in a-IGZO Thin-Film Transistors Fabricated at Low Temperature for Next-Generation Display. *J Electronic Materials* 2013; 42: 711-5.
- [16] Mativenga M, Seok M, Jang J. Gate bias-stress induced hump-effect in transfer characteristics of amorphous-indium-gallium-zinc-oxide thin-film transistors with various channel widths. *Appl Phys Lett* 2011; 99: 122107.
- [17] Nomura K, Kamiya T, Hosono H. Highly stable amorphous In-Ga-Zn-O thin-film transistors produced by eliminating deep subgap defects. *Appl Phys Lett* 2011; 99: 053505.
- [18] Chen TC, Chang TC, Hsieh TY, Lu WS, Jian FY, Tsai TM. Investigating the degradation behavior caused by charge trapping effect under DC and AC gate-bias stress for InGaZnO thin film transistor. *Appl Phys Lett* 2011; 99:022104.
- [19] Chowdhury DH, Migliorato P, Jang J. *Phys Lett* 2010; 97: 173506.
- [20] Jeon JH, Kim J, Ryu MK. Instability of an Amorphous Indium Gallium Zinc Oxide TFT under Bias and Light Illumination. *J Korean Phys Soc* 2011; 58: 158-62.

- [21] Vemuri RNP, Mathews WP, Marrs M, Alford TL. Investigation of defect generation and annihilation in IGZO TFTs during practical stress conditions: illumination and electrical bias. *J Phys D: Appl Phys* 2013; 46: 045101.
- [22] SILVACO-TCAD, ATLAS User's Manual: Device simulation software. SILVACO International, California: 2013.
- [23] Fung TC, Chuang C S, Chen C, Abe K, Cottle R, Townsend M. Two-dimensional numerical simulation of radio frequency sputter amorphous In-Ga-Zn-O thin-film transistors. *J Appl Phys* 2009; 106: 084511.
- [24] Chang Eun K, Cho E N, Moon P, Kim GH, Kim DL, Kim HJ. Density-of-States Modeling of Solution-Processed InGaZnO Thin-Film Transistors. *IEEE Electron Dev Lett* 2010; 31: 1131-3.
- [25] Kamiya T, Nomura K, Hosono H. Origins of High Mobility and Low Operation Voltage of Amorphous Oxide TFTs: Electronic Structure, Electron Transport, Defects and Doping. *J Display Technol* 2009; 5: 468-83.
- [26] Noh JY, Kim H, Nahm HH, Kim YS, Kim DH, Ahn BD. Cation composition effects on electronic structures of In-Sn-Zn-O amorphous semiconductors. *J Appl Phys* 2013; 113: 183706.
- [27] Hosono H. Material characteristics and applications of transparent amorphous oxide semiconductors, *NPG Asia Mater* 2010; 2(1): 15-22.
- [28] Kamiya T, Nomura K, Hosono H. Electronic structure of the amorphous oxide semiconductor $a\text{-InGaZnO}_{4-x}$: Tauc-Lorentz optical model and origins of subgap states. *Phys Status Solidi* 2009; A 206: 860-7.

- [29] Nomura K, Kamiya T, Yanagi H, Ikenaga E, Yang K, Kobayashi K. Subgap states in transparent amorphous oxide semiconductor, In-Ga-Zn-O, observed by bulk sensitive x-ray photoelectron spectroscopy. *Appl Phys Lett* 2008; 92: 202117.
- [30] Hsieh HH, Kamiya T, Nomura K, Hosono H, Wu V. Modeling of amorphous InGaZnO₄ thin film transistors and their subgap density of states. *Appl Phys Lett* 2008; 92: 133503.
- [31] Kimura M, Nakanishi T, Nomura K, Kamiya T, Hosono H. Trap densities in amorphous InGaZnO₄ thin-film transistors. *Appl Phys Lett* 2008; 92: 133512.
- [32] Sze SM. *Physics of Semiconductor Devices*. 2nd ed. New York: John Wiley and Sons, 1982.
- [33] Shockley W, Read WT. Statistics of the recombination of holes and electrons. *Phys Rev* 1952; 87: 835-42.
- [34] Hall RN. Electron-hole recombination in germanium. *Phys Rev* 1952; 87:387.
- [35] Meftah AM, Meftah AF, Hiouani F, Merazga A. Numerical simulation of the defect density influence on the steady state response of a silicon-based p-i-n cell. *J Phys: condens Matter* 2004; 16: 2003-16.
- [36] Park JH, Jeon K, Lee S, Kim S, Song I. Extraction of Density of States in Amorphous GaInZnO Thin-Film Transistors by Combining an Optical Charge Pumping and Capacitance-Voltage Characteristics. *IEEE Electron Dev Lett* 2008; 29: 1292-5.

Table captions

Table 1

The parameters of the DOS model in a-IGZO adopted in this work for the pre-stressed TFT. Note the absence of the acceptor-like Gaussian states.

Table 2

The parameters of the discrete acceptor-like trap created by stress at the semiconductor-insulator interface.

Table 3

The parameters of the Gaussian defects created by stress at the interface between the gate dielectric (SiO_2) and the semiconductor channel (a-IGZO).

Table 4

The parameters of the Gaussian defects created by stress in the gap of the semiconductor (a-IGZO).

Figure captions

Figure 1

A two dimensional view of the a-IGZO TFT structure simulated in this work [24].

Figure 2

The defect states representation within the band gap of disordered materials.

Figure 3

The simulated transfer characteristics of the TFT with the fixed charge states in the insulator dielectric (SiO_2) as a parameter. The density of these states increases from the initial value of $Q_f = 1 \times 10^{10} \text{ cm}^{-2}$ to $Q_f = 5 \times 10^{12} \text{ cm}^{-2}$.

Figure 4

The energy band diagram of the semiconductor-insulator interface for $Q_f = 1 \times 10^{10} \text{ cm}^{-2}$ (a) and $Q_f = 1 \times 10^{12} \text{ cm}^{-2}$ (b) at the same bias $V_g = 1.15 \text{ V}$.

Figure 5

The simulated transfer characteristics of the TFT with the discrete defect at the semiconductor-insulator interface as a parameter. The density of these states increases from the initial value of $N_{it} = 1 \times 10^{12} \text{ cm}^{-2}$ to $N_{it} = 1 \times 10^{14} \text{ cm}^{-2}$.

Figure 6

The simulated transfer characteristics of the TFT with a Gaussian distributed defect at the semiconductor-insulator interface for the acceptor-like and donor-like (a and b, respectively). The density of these states increases from $1 \times 10^{10} \text{ cm}^{-3} \text{ eV}^{-1}$ to $5 \times 10^{12} \text{ cm}^{-3} \text{ eV}^{-1}$.

Figure 7

The energy band diagram of the semiconductor-insulator interface for Gaussian acceptor-like distributed at the semiconductor-insulator interface with densities of $1 \times 10^{10} \text{ cm}^{-3} \text{ eV}^{-1}$ (a) and $5 \times 10^{12} \text{ cm}^{-3} \text{ eV}^{-1}$ (b) at the same bias $V_g = 1.15 \text{ V}$.

Figure 8

The energy band diagram of the semiconductor-insulator interface for Gaussian donor-like distributed at the semiconductor-insulator interface with densities of $1 \times 10^{10} \text{ cm}^{-3} \text{ eV}^{-1}$ (a) and $5 \times 10^{12} \text{ cm}^{-3} \text{ eV}^{-1}$ (b) at the same bias $V_g = 1.15 \text{ V}$.

Figure 9

The simulated transfer characteristics of the TFT with Gaussian distributed acceptor-like and donor-like (a and b, respectively) defect in the semiconductor band gap. The density of these states increases from $1 \times 10^{16} \text{ cm}^{-3} \text{ eV}^{-1}$ to $1 \times 10^{18} \text{ cm}^{-3} \text{ eV}^{-1}$.

Figure 10

The energy band diagram of the semiconductor-insulator interface for densities of the Gaussian acceptor-like distribution defect in the semiconductor gap of $1 \times 10^{17} \text{ cm}^{-3} \text{ eV}^{-1}$ (a) and $1 \times 10^{18} \text{ cm}^{-3} \text{ eV}^{-1}$ (b) at the same bias $V_g = 1.15 \text{ V}$.

Figure 11

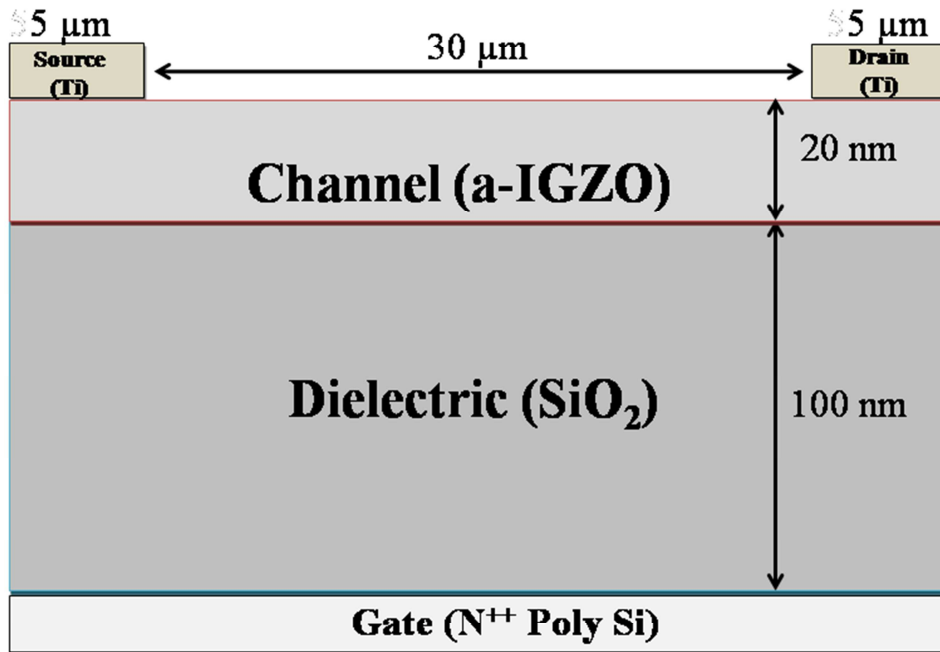
The energy band diagram of the semiconductor-insulator interface for densities of the Gaussian donor-like distribution defect in the semiconductor gap of $1 \times 10^{16} \text{ cm}^{-3} \text{ eV}^{-1}$ (a) and $1 \times 10^{18} \text{ cm}^{-3} \text{ eV}^{-1}$ (b) at the same bias $V_g = 1.15 \text{ V}$.

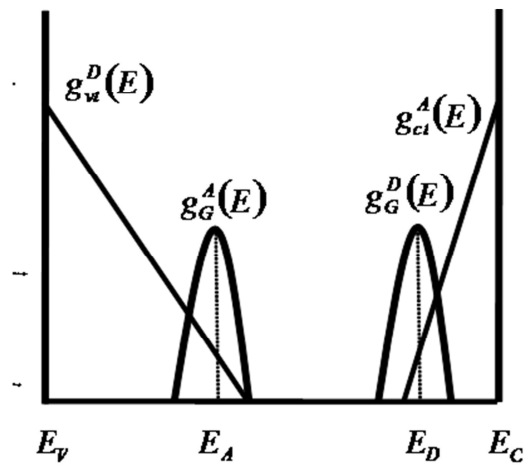
Parameter	Designation	Value
$g_{ta} \text{ (cm}^{-3}\text{eV}^{-1}\text{)}$	Effective density at E_C	1.55×10^{20}
$E_a \text{ (eV)}$	Characteristic slope energy of CB tail states	0.013
$g_{td} \text{ (cm}^{-3}\text{eV}^{-1}\text{)}$	Effective density at E_V	1.55×10^{20}
$E_d \text{ (eV)}$	Characteristic slope energy of VB tail states	0.12
$\sigma_{te} \text{ (cm}^2\text{)}$	Capture cross section of electrons by tail states	10^{-15}
$\sigma_{th} \text{ (cm}^2\text{)}$	Capture cross section of holes by tail states	10^{-15}
$g_{gd} \text{ (cm}^{-3}\text{eV}^{-1}\text{)}$	Total density of the donor-like Gaussian states	6.5×10^{16}
$E_D \text{ (eV)}$	Peak position of the donor-like Gaussian states	2.9
$\sigma_D \text{ (eV)}$	Standard deviation of the Gaussian distribution	0.1
$\sigma_{De} \text{ (cm}^2\text{)}$	Capture cross section of electrons by Gaussian states	10^{-15}
$\sigma_{Dh} \text{ (cm}^2\text{)}$	Capture cross section of holes by Gaussian states	10^{-15}

Parameter	Designation	Value
E_t (eV)	Acceptor/Donor trap position	0.4
N_t (cm ⁻²)	Acceptor/Donor trap density	Variable
σ_{tre} (cm ²)	Capture cross section of electrons by the acceptor/donor trap	10 ⁻¹³
σ_{trh} (cm ²)	Capture cross section of holes by the acceptor/donor trap	10 ⁻¹⁴

Parameter	Designation	Value
$g_{gd,ai}$ ($\text{cm}^{-3} \text{eV}^{-1}$)	Total density of the donor, acceptor-like Gaussian states at the interface	Variable
$E_{D,Ai}$ (eV)	Peak position of the donor, acceptor-like Gaussian states at the interface	2.9, 1
$\sigma_{D,Ai}$ (eV)	Standard deviation of the donor, acceptor-like Gaussian distribution at the interface	0.1, 0.5
$\sigma_{D,Aei}$ (cm^2)	Capture cross section of electrons by donor, acceptor-like Gaussian states at the interface	10^{-15}
$\sigma_{D,Ahi}$ (cm^2)	Capture cross section of holes by donor, acceptor-like Gaussian states at the interface	10^{-15}

Parameters	Designation	Value
$g_{gd,a}$ ($\text{cm}^{-3}\text{eV}^{-1}$)	Total density of the donor, acceptor-like Gaussian states	Variable
$E_{D,A}$ (eV)	Peak position of the donor, acceptor-like Gaussian states	2.9, 1
$\sigma_{D,A}$ (eV)	Standard deviation of the donor, acceptor-like Gaussian	0.1, 0.5
$\sigma_{D,Ae}$ (cm^2)	Capture cross section of electrons by donor, acceptor-like Gaussian	10^{-15}
$\sigma_{D,Ah}$ (cm^2)	Capture cross section of holes by the donor, acceptor-like Gaussian	10^{-15}





ACCEPTED MANUSCRIPT

